Study of OpenFOAM® Efficiency for Solving Fluid–Structure Interaction Problems

Matvey Kraposhin, Ksenia Kuzmina, Ilia Marchevsky and Valeria Puzikova

Abstract In the present research, the well-known test FSI problem of wind resonance phenomenon simulation for a circular cylinder is considered. It is well-investigated, both experimentally and numerically (Chen et al. in Phys Fluids 2011, [3]), for a wide range of parameters: Reynolds number, airfoil surface roughness, incident flow turbulence, etc. In this research, the simplest case is considered, in which the roughness influence is neglected and the incident flow is assumed to be laminar. Several numerical codes, both commercial and open source, can be used for simulating airfoil oscillations in the flow. Four numerical methods and the corresponding open-source codes are considered: the finite volume method with deformable mesh in `OpenFOAM`®; the particle finite element method with deformable mesh in the `Kratos` software; the meshfree Lagrangian vortex element method; and the LS-STAG immersed boundary method. The last two methods are implemented as in-house numerical codes. A comparison is carried out for the efficiency analysis of these methods and their implementations. It is shown that using `OpenFOAM`® is preferable for numerical simulations with FSI problems similar to the ones presented here, in which the investigation of system behavior within a wide range of parameters is required.

M. Kraposhin
Institute for System Programming of the Russian Academy of Sciences,
Alexander Solzhenitsyn st., 25., 109004 Moscow, Russia
e-mail: m.kraposhin@ispras.ru

K. Kuzmina · I. Marchevsky (✉) · V. Puzikova
Bauman Moscow State Technical University,
2-nd Baumanskaya st., 5., 105005 Moscow, Russia
e-mail: iliamarchevsky@mail.ru

K. Kuzmina
e-mail: kuz-ksen-serg@yandex.ru

V. Puzikova
e-mail: valeria.puzikova@gmail.com

J. M. Nóbrega and H. Jasak (eds.), *OpenFOAM*®,
https://doi.org/10.1007/978-3-319-60846-4_33

1 Introduction

In a number of engineering applications, bodies are immersed in a gas or fluid flow and exposed to aerohydrodynamic loads. Fully coupled 3D fluid–structure interaction (FSI) problems are extremely complicated, both from the mathematical and computational points of view. In many practical cases, the average density of the immersed body is higher than the density of the flow, thus it is possible to apply a well-known "splitting" approach, in which a single time step is divided into at least two substeps. During the first substep, a semi-implicit scheme, for which body motion parameters are assumed to be known, is used while simulating the flow around the body. During the second substep, an explicit scheme is used for body motion simulation under known hydrodynamic loads.

In practice, we often deal with extruded structures (with high elongation), so as a rough approximation, we consider this to be a 2D problem of interaction between the flow and the corresponding airfoil. This approach is particularly applicable when the airfoil cross section has angle points (points, at which the camber line of the airfoil loses its smoothness) and sharp edges. This approach is also accurate enough for FSI problems with bluff bodies that have smooth cross-sectional shapes, for example, flows around cylindrical rods, or pipes. Such bodies oscillate under von-Karman vortex shedding, and frequency-lock phenomenon takes place, which leads to similar flows around different cross sections.

In order to compare different numerical methods and computational codes for analyzing FSI problems, a simple test case considering the resonance of a circular cylinder inside the flow is proposed (Fig. 1).

The most interesting case of this phenomenon corresponds to the situation in which the eigenfrequency of the system is close to the von-Karman vortex shedding frequency. This phenomenon has been well-investigated, both experimentally and numerically, for a wide range of parameters: Reynolds number, airfoil surface roughness, incident flow turbulence, etc.

We consider the simplest case, in which we neglect the influence of surface roughness and the incident flow is assumed to be laminar. Four numerical methods and the corresponding open-source codes have been used: the finite volume method

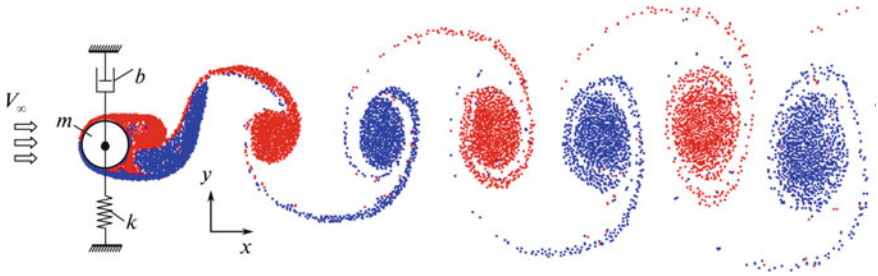

Fig. 1 Circular airfoil in a flow under viscoelastic constraints with a vortex wake behind it

(FVM) [9] with deformable mesh in `OpenFOAM®` [26, 30]; the particle finite element method (PFEM) [10, 11] with deformable mesh in the `Kratos` software [16]; the meshfree Lagrangian vortex element method (VEM) [5, 22]; and the level-set staggered mesh immersed boundary method (LS-STAG) [4]. The VEM and LS-STAG methods are implemented as in-house numerical codes.

2 Governing Equations

As mentioned before, the problem is considered to be a 2D unsteady case in which the flow around a cylindrical airfoil is viscous and incompressible. The continuity and momentum equations are as follows:

$$\nabla \cdot V = 0, \tag{1}$$

$$\frac{\partial V}{\partial t} + (V \cdot \nabla)V = -\nabla p + \frac{1}{\mathrm{Re}}\Delta V. \tag{2}$$

Here, $V = V(x, y, t) = u \cdot e_x + v \cdot e_y$ is the dimensionless velocity and $p = p(x, y, t)$ is the dimensionless pressure. The boundary conditions for the velocity field are defined as

$$V\big|_{\text{inlet}} = V_\infty, \qquad V\big|_{\text{airfoil}} = V^{\text{ib}}, \qquad \frac{\partial V}{\partial n}\Big|_{\text{outlet}} = 0. \tag{3}$$

Here, V^{ib} is the immersed boundary velocity. The airfoil is assumed to be rigid.

In order to simulate the wind resonance phenomenon, we consider one degree of freedom motion of the circular airfoil of diameter D across the stream. Constraint of the airfoil motion is assumed to be of the Kelvin–Voigt type (linear viscoelastic, Fig. 1) described by the following ordinary differential equation:

$$m\ddot{y} + b\dot{y} + ky = F_y. \tag{4}$$

Here, m is the airfoil mass, b is a small damping factor, k is the elasticity coefficient of the constraint, F_y is the lift force, and y is the deviation from the equilibrium state. The natural frequency of the system $\omega \approx \sqrt{k/m}$ can be changed by varying the elasticity coefficient k. The deviation from the equilibrium state on the n-th step of computation is $y^n = Y_C^n - Y_C^0$, where Y_C^0 is the coordinate of the airfoil center at the initial time and Y_C^n is its coordinate at the n-th step of computation. Numerical integration of the motion equation (4) was performed using the explicit 2nd order Runge–Kutta method

$$y^* = y^n + v_y^n \frac{\Delta t}{2}, \quad v_y^* = v_y^n + \frac{F_y - b v_y^n - k y^n}{m} \frac{\Delta t}{2}.$$
$$y^{n+1} = y^n + v_y^* \Delta t, \quad v_y^{n+1} = v_y^n + \frac{F_y - b v_y^* - k y^*}{m} \Delta t.$$

Here, v_y is the airfoil vertical velocity and "$*$" denotes values at the half of the time step.

3 Numerical Methods

Here, we briefly describe the numerical methods implemented and used for numerical simulations of the previously mentioned FSI problems. For more details regarding the described methods, please see [4, 5, 9–11, 16, 22–24, 26, 30].

3.1 OpenFOAM®: A Fluid–Structure Interaction Analysis Using the Finite Volume Method

A flow simulation with moving mesh is performed using the `pimpleDyMFoam` application implemented in `OpenFOAM®` [26]. The application allows for simulations of laminar and turbulent incompressible flows with prescribed boundary motion. In order to solve FSI problems, a special `function object` was implemented. It provides a weak coupling strategy between the fluid and the structure (Fig. 2), which includes the following steps:

1. Calculation of hydrodynamic forces exerted on the airfoil from the fluid.
2. Numerical integration of the motion equation of the structure under hydrodynamic forces.
3. Application of the airfoil camber line motion law to the boundary of the fluid domain.

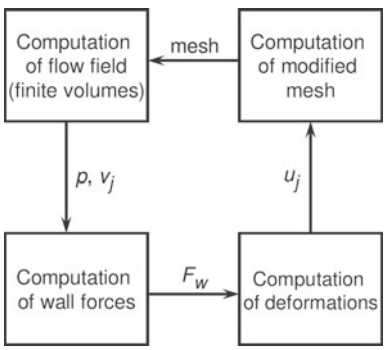

Fig. 2 Scheme of momentum exchange during the fluid–structure interaction process

The current implementation [15] of this `function object` allows for the simulation of airfoil motion with one degree of freedom (oscillations across the stream).

3.2 Kratos: Particle Finite Element Method with Fixed Mesh

This method belongs to the hybrid Lagrangian–Eulerian methods, and its recent modification PFEM2 allows for the use of a fixed mesh and large time steps. The convection of the fluid is taken into account via the motion of the Lagrangian particles, which are viewed as material points of the flow that can freely move in the flow region through the cells of the fixed mesh. In practice, this means that instead of solving the Navier–Stokes equation (2), we solve the equation with the material derivative

$$\frac{dV}{dt} = -\nabla p + \frac{1}{\mathrm{Re}}\Delta V.$$

Using this method, it is possible to simulate multidisciplinary and multiphase problems, in particular, flows with a free surface. In this case, particles can even separate from the main flow domain, representing, for instance, water drops.

When the convective substep is finished, the particle data are projected to the background fixed mesh, and the standard Finite Element-based approach is used to take into account the other terms of the Navier–Stokes equation (2). In order to satisfy the continuity equation, fractional step solvers [10] or monolithic solvers [1] can be used.

3.3 Vortex Element Method

Navier–Stokes equations (2) can be written down in Helmholtz form with respect to the vorticity field $\Omega(r,\ t) = \nabla \times V(r,\ t)$

$$\frac{\partial \Omega}{\partial t} + \nabla \times (\Omega \times U) = 0. \tag{5}$$

Here, $U(r, t) = V(r, t) + W(r, t)$, $W(r, t)$ is the so-called "diffusive velocity" [7], which is proportional to the viscosity coefficient

$$W(r, t) = \nu \frac{(\nabla \times \Omega) \times \Omega}{|\Omega|^2}. \tag{6}$$

If vorticity distribution is known, the flow velocity can be reconstructed by using the Biot–Savart law

$$V(r) = V_\infty + \frac{1}{2\pi}\int_S \frac{\Omega(\xi,t)\times(r-\xi)}{|r-\xi|^2}dS. \tag{7}$$

In order to compute the pressure distribution and hydrodynamic forces exerted on the airfoil, the analog of Bernoulli and Cauchy–Lagrange integrals is used [6].

Equation (5) describes vorticity transport in the flow with velocity U. "New" vorticity is generated only as a vortex sheet on the surface line of the airfoil, and its intensity $\gamma(\xi)$ can be found from the boundary condition on the airfoil's surface.

The vortex element method is a meshless particle-type method, so the vorticity field in the flow is discretized into separate vortex elements. Each vortex element is described by its position r_i and circulation Γ_i, $i = 1,\ldots,N$, where N is the number of vortex elements in the flow. So, the discretized Biot–Savart law has the following form:

$$V(r) = V_\infty + \sum_{i=1}^{N}\frac{\Gamma_i}{2\pi}\frac{k\times(r-r_i)}{|r-r_i|^2} + \oint_K \frac{k\times(r-\xi)}{2\pi|r-\xi|^2}\gamma(\xi)\,dl_\xi. \tag{8}$$

Here, k is the unit vector of the axis, which is orthogonal to the plane of the flow.

The movement of the vortex elements according to (5) is simulated via solution of the following ordinary differential equations system:

$$\frac{dr_i}{dt} = V(r_i) + W(r_i), \quad i = 1,\ldots,N. \tag{9}$$

The number of vortex elements in the flow N changes at every time step due to the vorticity flux from the surface line of the airfoil, which, in turn, is simulated by the vortex element generation near the airfoil. Their circulation is calculated from the vortex sheet intensity $\gamma(\xi)$ on the airfoil surface line. The circulation of all vortex elements in the flow remains constant and it can change only through a special numerical procedure of vortex wake restructuring that allows for the merging of closely spaced vortex elements and lowers their number in the flow.

Vortex sheet intensity $\gamma(\xi)$ can be found from the following boundary condition:

$$V(r) = V^{\text{ib}}(r), \quad r \in K. \tag{10}$$

This boundary condition can be reduced either to a singular integral equation of the first kind (in "classical" numerical schemes of a vortex method, see [5, 7, 21]) or to a Fredholm-type integral equation of the second kind with bounded (for smooth airfoils) kernel [12]

$$\oint_K \frac{[k\times(r-\xi)]\cdot\tau(r)}{2\pi|r-\xi|^2}\gamma(\xi)dl_\xi - \frac{\gamma(r)}{2} = -\tau(r)\cdot\left(V_\infty - V^{\text{ib}}(r) + \sum_{i=1}^{N}\frac{\Gamma_i}{2\pi}\frac{k\times(r-r_i)}{|r-r_i|^2}\right). \tag{11}$$

The solution to Eq. (11) is nonunique, so we need an additional condition for total vortex sheet circulation

$$\oint_K \gamma(r) dl_r = G. \tag{12}$$

There are high-accuracy numerical schemes developed for the numerical solution of Eqs. (11–12), which allow for the reduction of these equations to a linear algebraic equations system with well-conditioned matrix [17, 18]. By using these schemes, accuracy increases significantly [22]: in some cases, the error becomes one or even two orders of magnitude smaller in comparison with the classical schemes. As a result, this makes it possible to simulate FSI problems with high resolution.

It should be noted that the computational cost of simulating fixed and movable rigid airfoils when using the vortex element method remains nearly the same [19], so they are suitable for coupled FSI problems. However, vortex element movement simulation is an "N-body"-type problem [8], so special acceleration algorithms should be implemented. The well-known Barnes–Hut fast algorithm analog [8] can be very effective, especially when using an accurate analytical estimate of its computational cost [20], which allows for the choice of optimal parameters. Parallel computation algorithms are also used in order to reduce the computational time [19, 20].

3.4 LS-STAG Method

The LS-STAG immersed boundary method is a Eulerian method based on the finite volume approach. The fixed Cartesian mesh with cells $\Omega_{i,j} = (x_{i-1}, x_i) \times (y_{j-1}, y_j)$ and faces $\Gamma_{i,j}$ is introduced in the rectangular computational domain. Pressure $p_{i,j}$ and normal stresses are computed at centers $x^c_{i,j} = (x^c_i, y^c_j)$ of these cells. Unknown components $u_{i,j}$ and $v_{i,j}$ of velocity vector v are computed at the face center of the fluid mesh cell. These points are the centers of finite volumes of the staggered x-mesh and y-mesh: $\Omega^u_{i,j} = (x^c_i, x^c_{i+1}) \times (y_{j-1}, y_j)$ and $\Omega^v_{i,j} = (x_{i-1}, x_i) \times (y^c_j, y^c_{j+1})$, with faces $\Gamma^u_{i,j}$ and $\Gamma^v_{i,j}$, respectively. Shear stresses are computed at the corners of the base mesh (Fig. 3).

The fourth xy-mesh with cell centers in the corners of the base mesh is introduced for the simulation of turbulent flows. It is possible to simulate high Reynolds turbulent flows by using RANS, LES and DES approaches with Spalart–Allmaras, $k-\varepsilon$, $k-\omega$, and $k-\omega$ SST models [29].

The level-set function $\varphi = \varphi(x, y)$ [27] is used for capturing the airfoil immersed boundary Γ^{ib} [4]. The cells that the immersed boundary intersects are the so-called "cut-cells". These cells contain both the solid and liquid parts. The boundary Γ^{ib} is represented by a line segment on the cut-cell $\Omega_{i,j}$. In 2D cases, the cut-cells can be classified into trapezoidal, triangular and pentagonal cells. Examples of each type of cut-cell are presented in Fig. 4. The hydrodynamic force exerted on the airfoil can be computed by integrating the pressure distribution and shear stresses along the camber line of the airfoil.

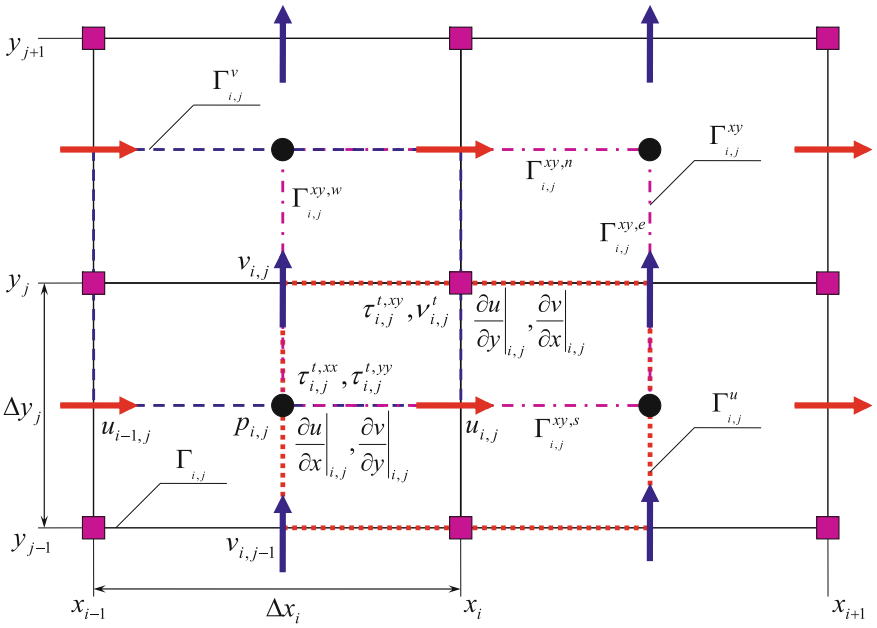

Fig. 3 Staggered arrangement of the variables on the LS-STAG mesh

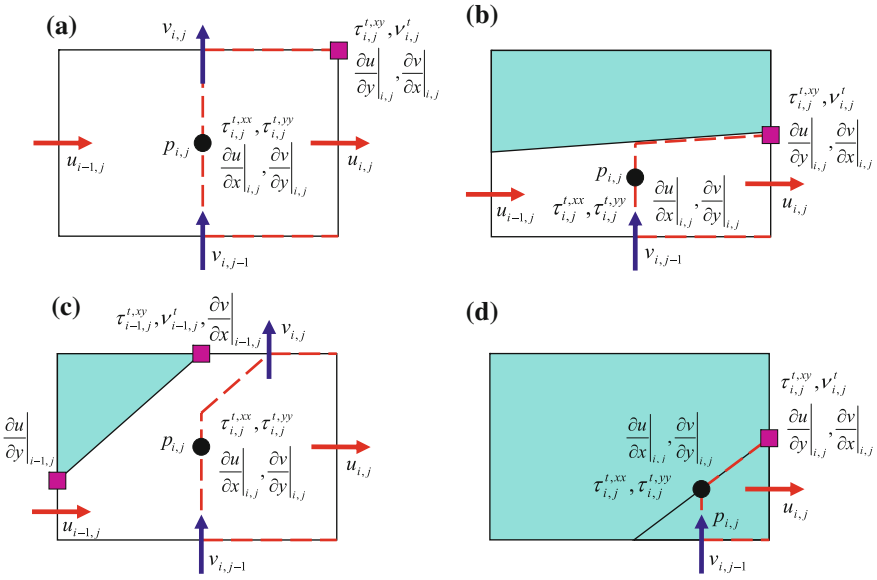

Fig. 4 Location of the variables' discretization points on the LS-STAG mesh: **a**—Cartesian Fluid Cell; **b**—North Trapezoidal Cell; **c**—Northwest Pentagonal Cell; **d**—Northwest Triangle Cell

According to the concept of the LS-STAG method [4], the governing equations (1–2) should be written in integral form for cells of base mesh, cells of x-mesh, and cells of y-mesh, respectively.

$$\begin{aligned}
&\int_{\Gamma_{i,j}} v \cdot n \, dS = 0, \\
&\frac{d}{dt} \int_{\Omega^u_{i,j}} u \, dV + \int_{\Gamma^u_{i,j}} (v \cdot n) u \, dS + \int_{\Gamma^u_{i,j}} p e_x \cdot n \, dS - \int_{\Gamma^u_{i,j}} \nu \nabla u \cdot n \, dS = 0, \\
&\frac{d}{dt} \int_{\Omega^v_{i,j}} v \, dV + \int_{\Gamma^v_{i,j}} (v \cdot n) v \, dS + \int_{\Gamma^v_{i,j}} p e_y \cdot n \, dS - \int_{\Gamma^v_{i,j}} \nu \nabla v \cdot n \, dS = 0. \quad (13)
\end{aligned}$$

Transport equations that correspond to turbulence model equations are being integrated over cells of the xy-mesh.

The time integration of the differential algebraic system that corresponds to a semi-discrete analog of the governing equations (1–2) is performed with a semi-implicit Euler scheme. The predictor step leads to discrete analogs of the Helmholtz equation for velocity prediction, while the corrector step leads to a discrete analog of the Poisson equation for pressure correction. The resulting linear systems are solved by using the FGMRES method with the ILU- and multigrid [31] preconditioning. The optimal parameters of the multigrid preconditioner were chosen by using the original algorithm for estimation of the solver cost-coefficient [25].

4 Numerical Simulation

We consider a viscous incompressible flow with low Reynolds number $\mathrm{Re} = 150$, i.e., the flow is laminar and a turbulence model is not needed. In dimensionless variables, the cylinder has unit diameter, the media has unit density, and the velocity of the incident flow is $V_\infty = 3$. The mass of the cylinder is $m = 39.15$. The fixed cylinder generates periodical vortex shedding in a quasi-steady regime with frequency f, which corresponds to the Strouhal number $\mathrm{Sh} = f d / V_\infty \approx 0.185$. Therefore, we choose the rigidity of the elastic constraint, so that the dimensionless construction frequency

$$\mathrm{Sh}_\omega = \frac{1}{2\pi} \sqrt{\frac{k}{m}} \frac{d}{V_\infty}$$

varies within the range $0.160 \ldots 0.220$. The viscosity of the constraint has a small value, $b = 0.731$, and it practically does not influence the eigenvalue of the system at all. The rest of the system parameters were chosen in the same way as in [13].

Table 1 Results of flow simulation around fixed cylinder

	C_{xa}	Sh	C_{ya}^{ampl}
Experiment	1.15 . . . 1.45	0.175 . . . 0.195	0.50 . . . 0.65
`OpenFOAM®`	1.44	0.190	0.60
`Kratos`	1.20	0.190	0.53
Vortex method	1.31	0.177	0.51
LS-STAG	1.32	0.191	0.63

4.1 Flow Simulation Around the Fixed Airfoil

The described numerical methods were first validated by using a classical test problem of flow around an immovable airfoil. At the beginning of the numerical simulation, the incident flow velocity was set to zero, and the flow was gradually accelerated, until its value reached $V_\infty = 3$. During the simulation, the dimensionless drag coefficient, the amplitude of the lift coefficient and the vortex shedding frequency was measured. The results are shown in Table 1.

Calculations show that all the methods give reasonable results compared to the experimental data. At the same time, it is necessary to notice that the Particle Finite Element Method (PFEM2) implemented in the `Kratos` software overpredicts the pressure values near the critical point compared to the experiment.

Mesh motion in `OpenFOAM®` is calculated by solving the point displacement Laplacian equation. This type of numerical implementation is efficient only for simple airfoil motion trajectory—displacements with a small rotation angle.

The LS-STAG method has potential in flow simulations around arbitrary moving airfoils with complicated shapes. However, its computational complexity is rather high. Unfortunately, its parallel implementation is not available at the moment (due to principal problems with matrix decompositions).

4.2 Wind Resonance Simulation

A number of numerical simulations have been carried out for different values of the dimensionless frequency in which the unsteady process has been simulated from $t = 0$ to $t = 200$. The obtained dependencies of the dimensionless oscillation amplitude A/d (in quasi-steady mode) of the airfoil on the dimensionless natural frequency of the system Sh_ω are shown in Fig. 5.

The obtained dependencies are very close, while they differ only in shift of frequency, which corresponds to the results of the Strouhal number (dimensionless vortex shedding frequency) computation for the fixed cylinder (see Table 1). The maximum value of the amplitude is close to the experimental value [2, 13].

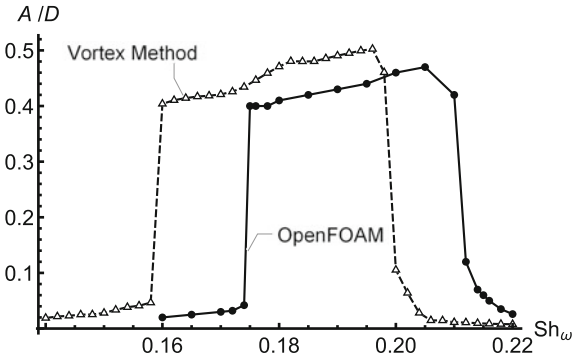

Fig. 5 Circular airfoil oscillations' amplitude dependence on the natural frequency of the system, obtained with the finite volume method (OpenFOAM®) and the vortex method

Table 2 Computational time (in hours) for OpenFOAM® and for the vortex method

	1 CPU	2 CPU	4 CPU	8 CPU	16 CPU
OpenFOAM®					
Far from resonance	58.1	36.0	24.3	15.5	9.8
Close to resonance	74.4	45.8	30.1	19.6	13.7
Vortex method					
Far from resonance	41.3	22.6	12.0	7.1	4.7
Close to resonance	63.4	34.7	17.9	10.1	6.6

The computational times spent for numerical simulations of the flow around freely oscillating airfoils by using OpenFOAM® and the vortex method is given in Table 2. Parallel computational technologies (MPI) reduce the required computational time significantly. Measured computational time is given for two regimes: close to wind resonance and far from it.

When solving the same problem by using the LS-STAG method in sequential mode, the time of computation was approximately 110 and 150 h for non-resonance and resonance cases, respectively; the time for non-resonance simulation in Kratos (PFEM2 method) was approximately 55 h in sequential mode and 16 h in parallel mode with OpenMP technology using 4 CPU cores. However, when simulating airfoil oscillations with rather high amplitude, the amplitude of the lift force coefficient in Kratos is much higher than in the experiment. Therefore, this method should be used only for simulations in which the amplitude of airfoil oscillations is not larger than several percent of the diameter size. The given results for all numerical methods were obtained on the same computational cluster consisting of 8 personal computers with Intel Core i7 3.2 GHz processors connected by Cisco Gigabit Ethernet.

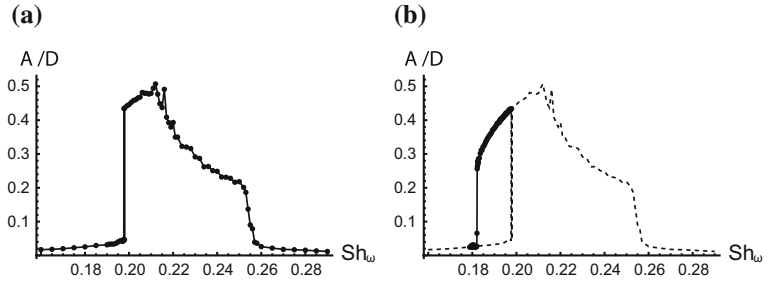

Fig. 6 Maximum amplitude of the circular airfoil oscillations simulated using the vortex element method: **a** airfoil's initial state in the equilibrium position, **b** airfoil's initial state is close to resonance oscillations

4.3 Hysteresis Simulation

In order to capture a well-known hysteresis phenomenon [14] during the flow around an airfoil with elastic constraints, 80 simulations with different dimensionless frequencies were performed. The Reynolds number was set to 1000, while the other parameters remained the same as in the previously stated resonance simulations. The dependency of the oscillations' amplitude on the natural frequency Sh_ω is shown in Fig. 6a, where a sharp amplitude increase is observed at $\mathrm{Sh}_\omega \approx 0.198$.

In the second series of numerical simulations, Sh_ω was equal to 0.21 from $t = 0$ to $t = 100$. During this time interval, the oscillations reached steady state with amplitude $A/D \approx 0.47$. At simulation time $t = 100$, the elasticity coefficient of the constraint was changed abruptly to the values that correspond to oscillation frequencies Sh_ω from 0.178 to 0.198. In each case, after the transitional period, new steady oscillations were reached. Their amplitudes are shown in Fig. 6b (dots connected by a solid line).

The obtained results for maximum oscillation amplitude, the resonance frequency and the hysteresis properties are in good agreement with the results given in [13, 14].

5 Comparison of the Considered Numerical Methods

A comparison of the properties between the considered numerical methods is presented in Table 3. The sign "+" means that this property is inherent in the method and is implemented efficiently; "±" means that the method yields to others in this feature; "−" means the absence of the property or its inefficient implementation; the asterisk "∗" means that this property is not fully implemented or it is in a development stage.

Unfortunately, it is impossible to use vortex methods and the particle finite element method when simulations of flows with high Reynolds numbers are required. In vortex methods in a purely Lagrangian framework, attempts to implement turbulence

Table 3 Comparison of the numerical methods

	OpenFOAM®	Vortex method	Kratos	LS-STAG
Computational cost	±	+	+	−
Accuracy	+	±	±	+
Airfoil motion	±	+	−	+
Parallel implementation	+	+	*	*
Automatic time step choice	+	*	−	±
Turbulent flows	+	−	−	+
3D flows	+	*	+	*

models are not very efficient [28]. The current implementation of the FEM particle model inside the Kratos software package does not have the required functionality for implementing turbulence models.

6 Conclusion

When simulating flows with relatively small Reynolds numbers (from 100 to 10,000), all the abovementioned numerical models give results that are in good agreement with the experimental data. The overall efficiencies of all considered methods and codes are comparable. However, simulating flows in high Reynolds regimes, in which turbulent effects must be taken into account while preserving acceptable computational costs, can be done only with OpenFOAM®. It should be noted, however, that the choice of the turbulence model, as well as that of the RANS/LES approach, is a nontrivial problem. Moreover, OpenFOAM® is well parallelized, thus computational time can be reduced significantly. At the same time, parallel algorithms in vortex methods are efficient only for a small number of computational cores. Current PFEM implementation in the Kratos software works in parallel mode only when using OpenMP technology (on shared-memory systems).

As a result, the following conclusion can be made: OpenFOAM® is a good tool for fast estimation of dynamic processes in fluid–structure interaction problems. It enables analysis of FSI system behavior within a wide range of parameters.

References

1. Becker, P., Idelsohn, S.R., Onate, E.: A unified monolithic approach for multi-fluid flows and fluid-structure interaction using the Particle Finite Element Method with fixed mesh. Computat.

Mech. (2015) https://doi.org/10.1007/s00466-014-1107-0
2. Blevins, R.D., Coughran, C.S.: Experimental investigation of vortex-induced vibration in one and two dimensions with variable mass, damping, and reynolds number. J. of Fluids Eng. (2009) https://doi.org/10.1115/1.3222904
3. Chen, S.-S., Yen, R.-H., Wang, A.-B.: Investigation of the resonant phenomenon of flow around a vibrating cylinder in a subcritical regime. Physics of Fluids (2011) https://doi.org/10.1063/1.3540673
4. Cheny, Y., Botella, O.: The LS-STAG method: A new immersed boundary/level-set method for the computation of incompressible viscous flows in complex moving geometries with good conservation properties. J. of Comput. Phys. (2010) https://doi.org/10.1016/j.jcp.2009.10.007
5. Cottet, G.-H., Koumoutsakos, P.D.: Vortex methods. Theory and practice. Cambridge University Press (2008)
6. Dynnikova, G.Ya.: Vortex motion in two-dimensional viscous fluid flows. Fluid Dynamics (2003) https://doi.org/10.1023/B:FLUI.0000007829.78673.01
7. Dynnikova, G.Ya.: The Lagrangian approach to solving the time-dependent Navier-Stokes equations. Dokl. Phys. (2004) https://doi.org/10.1134/1.1831530
8. Dynnikova, G.Ya.: Fast technique for solving the N-body problem in flow simulation by vortex methods. Comput. Math. and Math. Phys. (2009) https://doi.org/10.1134/S0965542509080090
9. Ferziger, J., Peric, M.: Computational methods for fluid dynamics. Springer (2002)
10. Idelsohn, S., Nigro, N., Gimenez, J., Rossi, R., Marti, J.: A fast and accurate method to solve the incompressible Navier-Stokes equations. Engineering Computations. (2013) https://doi.org/10.1108/02644401311304854
11. Idelsohn, S., Nigro, N., Limache, A., Onate, E.: Large time-step explicit integration method for solving problems with dominant convection. Comput. Methods. Appl. Mech. Eng. (2012) https://doi.org/10.1016/j.cma.2011.12.008
12. Kempka, S.N., Glass, M.W., Peery, J.S., Strickland, J.H.: Accuracy considerations for implementing velocity boundary conditions in vorticity formulations. SANDIA Report SAND96-0583 (1996)
13. Klamo, J.T., Leonard, A., Roshko, A.: On the maximum amplitude for a freely vibrating cylinder in cross flow. J. Fluids. Struct. (2005) https://doi.org/10.1016/j.jfluidstructs.2005.07.010
14. Klamo, J.T., Leonard, A., Roshko, A.: The effects of damping on the amplitude and frequency response of a freely vibrating cylinder in cross-flow. J. Fluids. Struct. (2006) https://doi.org/10.1016/j.jfluidstructs.2006.04.009
15. Kraposhin, M.V., Marchevsky, I.K.: Implementation of simple FSI model with functionObject (2016) https://doi.org/10.13140/RG.2.1.1526.6809/1 https://github.com/unicfdlab/TrainingTracks/tree/master/OpenFOAM/simpleFsi-OF3.0.0. Cited 1 Oct 2016
16. Kratos multi-physics. http://www.cimne.com/kratos. Cited 1 Oct 2016
17. Kuzmina, K.S., Marchevskii, I.K., Moreva, V.S.: Vortex Sheet Intensity Computation in Incompressible Flow Simulation Around an Airfoil by Using Vortex Methods. Math. Model. and Comput. Simul. (2018) https://doi.org/10.1134/S2070048218030092.
18. Kuz'mina, K.S., Marchevskii, I.K., Moreva, V.S., Ryatina, E.P.: Numerical scheme of the second order of accuracy for vortex methods for incompressible flow simulation around airfoils. Russian Aeronautics (2017) https://doi.org/10.3103/S1068799816030114
19. Kuzmina, K.S., Marchevsky, I.K., Moreva, V.S.: Parallel Implementation of Vortex Element Method on CPUs and GPUs. Procedia Computer Science (2015) https://doi.org/10.1016/j.procs.2015.11.010
20. Kuzmina, K., Marchevsky, I., Ryatina, E.: VM2D: Open source code for 2D incompressible flow simulation by using vortex methods. Commun. Comput. and Inf. Sci. (2018) https://doi.org/10.1007/978-3-319-99673-8_18
21. Lifanov, I.K., Belotserkovskii, S.M.: Methods of Discrete Vortices. CRC Press (1993)
22. Marchevsky, I.K., Moreva, V.S., Puzikova V.V.: The efficiency comparison of the vortex element method and the immersed boundary method for numerical simulation of airfoils hydroelastic oscillations COUPLED PROBLEMS 2015: Proc. of VI Int. Conf. on Computational Methods for Coupled Problems in Sci. and Eng., 800-811 (2015). http://congress.cimne.com/coupled2015/frontal/doc/EbookCOUPLED15.pdf. Cited 1 Oct 2016

23. Marchevskii, I.K., Puzikova V.V.: Numerical simulation of the flow around two fixed circular airfoils positioned in tandem using the LS-STAG method. J. Mach. Manuf. Reliab. (2016) https://doi.org/10.3103/S1052618816020084
24. Marchevskii, I.K., Puzikova V.V.: Numerical simulation of the flow around two circular airfoils positioned across the stream using the LS-STAG method. J. Mach. Manuf. Reliab. (2017) https://doi.org/10.3103/S105261881702011X
25. Marchevsky, I.K., Puzikova, V.V.: OpenFOAM® iterative methods efficiency analysis for linear systems solving. Proceedings of the Institute for System Programming of RAS (2013) https://doi.org/10.15514/ISPRAS-2013-24-4 [in Russian]
26. OpenFOAM® —the open source computational fluid dynamics (cfd) toolbox. http://www.openfoam.com. Cited 1 Oct 2016
27. Osher, S., Fedkiw, R.P.: Level set methods and dynamic implicit surfaces. Springer (2003)
28. Pereira, L.A.A., Hirata, M.H., Silveira Neto A.: Vortex method with turbulence sub-grid scale modelling. J. Braz. Soc. Mech. Sci. & Eng. (2003) https://doi.org/10.1590/S1678-58782003000200005
29. Puzikova, V.V.: Development of the LS-STAG immersed boundary method modification or mathematical modelling in coupled hydroelastic problems. Ph.D. dissertation, Bauman Moscow State Technical University, Russia (2016) [in Russian] http://mechmath.ipmnet.ru/lib/?s=thesis_mech. Cited 1 Oct 2016
30. Weller, H.G., Tabor, G., Jasak, H., Fureby, C.: A tensorial approach to computational continuum mechanics using object-oriented techniques. Computers in Physics (1998) https://doi.org/10.1063/1.168744
31. Wesseling, P.: An introduction to multigrid methods. John Willey & Sons Ltd. (1991)